J. Fluid Mech. (1990), *vol.* 211, *pp.* 73–93
Printed in Great Britain

Stability of the flow past a sphere

By INCHUL KIM† AND ARNE J. PEARLSTEIN†
Department of Aerospace and Mechanical Engineering, University of Arizona, Tucson, AZ 85721, USA

(Received 26 January 1989 and in revised form 13 July 1989)

Experiment shows that the steady axisymmetric flow past a sphere becomes unstable in the range $120 < Re < 300$. The resulting time-dependent non-axisymmetric flow gives rise to non-axisymmetric vortex shedding at higher Reynolds numbers. The present work reports a computational investigation of the linear stability of the steady axisymmetric base flow. We use a spectral technique to represent the base flow. We then perform a linear stability analysis with respect to axisymmetric and non-axisymmetric disturbances. A spectral technique similar to that employed in the base-flow calculation is used to solve the linear-disturbance equations in stream-function form (for axisymmetric disturbances), and in a modified primitive variables form (for non-axisymmetric disturbances). The analysis shows that the axisymmetric base flow undergoes a Hopf bifurcation at $Re = 175.1$, with the critical disturbance having azimuthal wavenumber $m = 1$, and dimensionless frequency (non-dimensionalized as a Strouhal number, St) 0.0955. The critical Re, azimuthal mode number, and St are favourably compared to previous experimental work.

1. Introduction

At sufficiently small Reynolds numbers, flow about bluff bodies is known to be attached and steady. At higher Reynolds numbers, the flow becomes separated, unsteady, and ultimately turbulent. The nature of this transition can have important consequences in a number of practical applications.

In recent years, the process by which this transition occurs has been extensively studied for two-dimensional bodies, both experimentally (Provansal, Mathis & Boyer 1987) and theoretically (Monkewitz & Nguyen 1987; Monkewitz 1988*a*). In the case of a circular cylinder (Thoman & Szewczyk 1969; Lin, Pepper & Lee 1976; Jackson 1987; Zebib 1987), the first stage in the transition is found to be a wake instability of the separated steady flow, leading to a time-periodic two-dimensional flow with considerable concentration of bound vorticity in the near wake adjacent to the body. As Re is increased, this flow may in turn give rise to the shedding of fluid parcels with concentrated vorticity ('vortex shedding'), and eventually to turbulence.

For axisymmetric bodies, the transition is less well understood, despite considerable experimental progress for wakes of slender (Hama & Peterson 1976; Peterson & Hama 1978; Sato & Okada 1966) and bluff (Achenbach 1974; Fuchs, Mercker & Michel 1979; Goldburg & Florsheim 1966; Jayaweera & Mason 1965; Kim & Durbin 1988; Masliyah 1972; Willmarth, Hawk & Harvey 1964) bodies of revolution. For non-spherical bodies of revolution, experiments may be plagued by

† Present address: Department of Mechanical and Industrial Engineering, University of Illinois at Urbana-Champaign, 1206 West Green Street, Urbana, IL 61801, USA.

the need for extremely precise alignment of the body's axis with the flow direction (Hama *et al.* 1977).

On the theoretical side, there have been several studies of the stability of axisymmetric parallel velocity profiles as models of axisymmetric wakes (Batchelor & Gill 1962; Gold 1963; Lessen & Singh 1973; Monkewitz 1988*b*). Batchelor & Gill performed inviscid stability analyses on parallel axisymmetric velocity profiles appropriate to jets and wakes, and found the critical azimuthal wavenumber to be $m = 1$. Gold extended this approach to compressible flows, and found the same critical value of m. Lessen & Singh extended the approach of Batchelor & Gill by including the viscous terms in the disturbance equations, and also found $m = 1$ to be the critical azimuthal wavenumber. More recently, Monkewitz (1988*b*) has also considered, on a viscous basis, the linear stability of incompressible axisymmetric parallel wake profiles, including those appropriate to bluff bodies of revolution. His results provide conditions under which these parallel flows are absolutely unstable with respect to $m = 1$ disturbances.

The prototypical axisymmetric flow is that generated by a sphere in a uniform flow. At low Reynolds numbers, the flow is steady, axisymmetric, and remains attached. In the classical experiments of Taneda (1956), separation is first observed at $Re \approx 24$. (All Reynolds numbers referred to herein are based on diameter.) As Re increases, the downstream extent of the recirculating wake progressively increases, and the separation circle on the sphere moves forward from the rear stagnation point. At values of Re in the range $120 < Re < 300$, experiment shows that the steady axisymmetric flow loses its stability (henceforth referred to as the first transition, with corresponding Reynolds number Re_1) and the motion becomes unsteady and non-axisymmetric. There is considerable uncertainty in the experimental value of Re_1 (Goldburg & Florsheim 1966; Möller 1938; Nakamura 1976; Roos & Willmarth 1971; Taneda 1956; Toulcova & Podzimek 1968; Zikmundova 1970).

The experimental determination of Re_1 in conventional wind/water tunnel facilities is complicated by three factors. First, the presence of a sting or other support is known to have a strong influence on the stability of the sphere wake (Roos 1968; Roos & Willmarth 1971). This leads to the hypothesis (discussed in more detail in §4) that Re_1 depends rather delicately on the details of the base flow. Secondly, because instability sets in as a weak, low-frequency oscillation, the instability may not be easily discernible. Thirdly, free-stream turbulence is known to have a significant influence on the Reynolds number at which vortex shedding occurs (Zarin 1970), and may also affect Re_1. The first of these problems can be avoided by use of a magnetic suspension balance or some other non-interfering support (Zarin 1970). The third can be avoided by towing the sphere through otherwise quiescent fluid (Möller 1938; Roos & Willmarth 1971). The first problem can be avoided and the third can in large part be eliminated by using freely falling or rising spheres. Unfortunately, this introduces a possible coupling of the rigid body motion of the sphere to the non-axisymmetric instability of the wake (through the no-slip boundary condition on the surface of the sphere). This may in turn lead to a reduction in Re_1 for freely falling/rising spheres. For either fixed or falling/rising spheres, the weakness of the oscillations at the onset of instability presents a formidable challenge to the experimental determination of Re_1.

The stability of the steady axisymmetric flow is especially important because the breakdown to non-axisymmetric (helical) vortex shedding at higher Re appears to occur via an intermediate stage involving non-axisymmetric wake oscillations. Although the recent work of Kim & Durbin (1988) has substantially clarified the previously muddled (Achenbach 1974; MacCready & Jex 1964; Möller 1938;

Preukschat 1962; Shafrir 1965; Sheth 1970; Stringham, Simons & Guy 1969; Viets 1971; Viets & Lee 1971) nature of the vortex shedding at higher Re, there is still relatively little known about the mechanism by which the transition from non-axisymmetric wake oscillations to vortex shedding occurs. Obviously, a first step in unravelling the transition process is the determination of the Re at which the first transition occurs.

It is the purpose of the present work to investigate computationally the first stage in the transition process for the geometrically simplest axisymmetric body, namely the sphere. In contrast to the work of Gold (1963), Lessen & Singh (1973) and Monkewitz (1988*b*), our work uses a numerically computed base flow which is a converged *non-parallel* solution of the Navier–Stokes equations. The disturbance equations are exact linearizations of the three-dimensional Navier–Stokes equations, with full treatment of the viscous and (on a linear basis) the inertial terms. To the best of our knowledge, this is the first three-dimensional stability analysis of a non-parallel axisymmetric viscous flow. The only previous attempt to compute Re_1 for a sphere is that of Kawaguti (1955). In that work, a Galerkin approximation to the steady axisymmetric solution was used as the base flow. A Galerkin calculation showed that the base flow became unstable with respect to *axisymmetric* disturbances at $Re_1 = 51$, which is at variance with both the range of experimentally determined Re_1, and with the non-axisymmetric nature of the flow above Re_1 (Kendall 1964; Goldburg & Florsheim 1966; Roos & Willmarth 1971).

The remainder of the paper is divided into four sections. In §2, we present the governing equations and briefly discuss the method by which the steady axisymmetric solution is computed. In §3, we present the linear stability analysis and results for axisymmetric and non-axisymmetric disturbances. In §4, we compare the computed results to previous experimental work. We conclude in §5 with a discussion of the results in terms of the development of flow around a sphere, and in the more general context of transition for axisymmetric bluff bodies.

2. Governing equations and the axisymmetric base flow

2.1. *Governing equations*

We consider the incompressible flow of a constant property Newtonian fluid past a fixed rigid sphere. Far from the sphere, the flow is uniform and has a constant velocity $\boldsymbol{U}_0$. We non-dimensionalize the Navier–Stokes equations using the sphere radius R_0 as the characteristic length, R_0/U_0 as the characteristic time, ρU_0^2 as the characteristic pressure, and $U_0 = |\boldsymbol{U}_0|$ as the characteristic velocity to get

$$\nabla \cdot \boldsymbol{u} = 0, \tag{2.1}$$

$$\frac{\partial \boldsymbol{u}}{\partial t} + (\boldsymbol{u} \cdot \nabla)\,\boldsymbol{u} = -\nabla p + \frac{2}{Re}\nabla^2 \boldsymbol{u}. \tag{2.2}$$

The flow satisfies the no-slip boundary condition

$$\boldsymbol{u}(1, \theta, \phi, t) = \boldsymbol{0}, \tag{2.3}$$

on the surface of the sphere.

2.2. *Base-flow calculation*

In order to conduct a proper analysis of the first transition for flow about a sphere, it is necessary to have a representation of the base flow which is useable in the stability analysis and is accurate. These two considerations have significant

implications for the calculation of the axisymmetric base flow, which we discuss in the present section.

First, the base flow must be compatible with the method used to solve the linear disturbance equations in the stability analysis. Secondly, since previous experimental work has shown the development of instability to be sensitively dependent on the details of the base flow in the wake region, it is crucial that the structure of the wake be accurately represented by the computed base flow.

We have chosen to solve the stability problem using spectral methods. Use of a spectral technique to compute the base flow offers several advantages over a finite difference approach (e.g. Fornberg 1988), including the elimination of interpolation and the numerical approximation of derivatives in the inertial terms of the linear disturbance equations. For reasons discussed separately (Kim 1989), the spectral method chosen to compute the steady axisymmetric flow is a modification of the technique used by Zebib (1984) for $Re = 1$, 5 and 10. The changes we have implemented allow the base-flow calculation to be efficiently extended to $Re = 200$, and for the convergence of the solutions to be clearly established. This method is entirely compatible with the stability analysis presented in §3.

Zebib's method employs a fourth-order stream-function formulation of the governing equations for steady axisymmetric flow in spherical coordinates. Briefly, the differences between our technique and Zebib's are as follows. We have decomposed the solution into a uniform flow and a Galerkin series, in which the ith angular trial function is an integral of the ith Legendre polynomial and has the proper symmetry (stream-function vanishes on $\theta = 0, \pi$). We have also used a correct asymptotic implementation of the 'soft' far-field conditions of Fornberg (1980) at the outer boundary of the computational domain. Finally, our Galerkin integrations are done with weightings of the form $r^k \sin\theta$. (We have used $k = 1$ herein; essentially identical results, requiring the same number of Newton iterations to solve the nonlinear algebraic equation system, are obtained for $k = 0, 1, 2$.)

With these improvements, we are able to compute the steady axisymmetric solution to Reynolds numbers in excess of Re_1. The convergence of the base flow over a wide range of Re has been established by detailed checks of various scalar properties, including the drag coefficient, dimensionless length of the separated flow region, and separation angle as both the size of the computational domain and the spatial resolution are increased. Details of the procedure, and a favourable comparison of the results to previous experimental work (Taneda 1956; Modi & Akutsu 1984), are discussed in detail in Kim & Pearlstein (1989). For subsequent reference, we denote by K and $L+1$ the number of polar and radial functions, respectively, retained in the base-flow expansion.

3. Linear stability analysis

We consider infinitesimally small disturbances to the steady axisymmetric flow and decompose the dimensionless velocity and pressure into

$$\boldsymbol{u}(r,\theta,\phi,t) = \boldsymbol{U}_s(r,\theta) + \boldsymbol{u}'(r,\theta,\phi,t),$$

$$p(r,\theta,\phi,t) = P_s(r,\theta) + p'(r,\theta,\phi,t),$$

where the subscript s denotes a base-flow quantity and the prime denotes a disturbance quantity. In what follows, we shall only retain terms to first order in the disturbance quantities.

The disturbances can be Fourier decomposed into azimuthal components according to

$$\boldsymbol{u}'(r,\theta,\phi,t) = \sum_{m=-\infty}^{\infty} \boldsymbol{u}_m(r,\theta,\phi,t) = \sum_{m=-\infty}^{\infty} \boldsymbol{u}'_m(r,\theta,t)\,\mathrm{e}^{\mathrm{i}m\phi}, \tag{3.1a}$$

and

$$p'(r,\theta,\phi,t) = \sum_{m=-\infty}^{\infty} p_m(r,\theta,\phi,t) = \sum_{m=-\infty}^{\infty} p'_m(r,\theta,t)\,\mathrm{e}^{\mathrm{i}m\phi}. \tag{3.1b}$$

The remainder of this section is devoted to discussions of the fates of axisymmetric ($m = 0$) and non-axisymmetric ($m \neq 0$) disturbances to the steady axisymmetric base flow. For each azimuthal wavenumber, we will then seek to determine whether, at fixed Re, any disturbances grow in time. The critical Reynolds number for the axisymmetric base flow, Re_1, is the Re for which no disturbances grow, and one or more disturbances are neutral. Unless otherwise indicated, the base-flow calculation was performed with $K = L = 28$.

3.1. *Axisymmetric ($m = 0$) disturbances*

We begin by considering axisymmetric disturbances with arbitrary time dependence. Because the base flow and disturbance are axisymmetric, we can use a stream-function formulation of the Navier–Stokes equations

$$\frac{\partial(\mathrm{D}^2\Psi')}{\partial t} + \frac{1}{r^2}\left\{\frac{\partial\Psi_s}{\partial r}\frac{\partial}{\partial\zeta} - \frac{\partial\Psi_s}{\partial\zeta}\frac{\partial}{\partial r} + \frac{2\zeta}{1-\zeta^2}\frac{\partial\Psi_s}{\partial r} + \frac{2}{r}\frac{\partial\Psi_s}{\partial\zeta}\right\}\mathrm{D}^2\Psi'$$
$$+ \frac{1}{r^2}\left\{\frac{\partial\Psi'}{\partial r}\frac{\partial}{\partial\zeta} - \frac{\partial\Psi'}{\partial\zeta}\frac{\partial}{\partial r} + \frac{2\zeta}{1-\zeta^2}\frac{\partial\Psi'}{\partial r} + \frac{2}{r}\frac{\partial\Psi'}{\partial\zeta}\right\}\mathrm{D}^2\Psi_s - \frac{2}{Re}\mathrm{D}^4\Psi' = 0, \tag{3.2}$$

with boundary conditions

$$\Psi'(1,\zeta,t) = 0, \quad \frac{\partial\Psi'(1,\zeta,t)}{\partial r} = 0. \tag{3.3a,b}$$

At large r, we have the asymptotic boundary condition

$$\lim_{r\to\infty} \Psi'(r,\zeta,t) \to 0. \tag{3.4}$$

In (3.2), we have defined $\zeta = \cos\theta$, and

$$\mathrm{D}^2 \equiv \frac{\partial^2}{\partial r^2} + \frac{1-\zeta^2}{r^2}\frac{\partial^2}{\partial\zeta^2}.$$

Since the solution must be symmetric about $\theta = 0$ and π, we also impose the conditions

$$\Psi'(r,1,t) = 0, \quad \Psi'(r,-1,t) = 0. \tag{3.5a,b}$$

The determination of Re_1 is thus equivalent to computing the largest value of Re for which no solution of (3.2)–(3.5) grows in time. As (3.2)–(3.5) are linear and time-invariant, we investigate modal solutions of the form

$$\Psi'(r,\zeta,t) = \psi(r,\zeta)\,\mathrm{e}^{\sigma t},$$

where σ is the temporal eigenvalue. Thus, we consider

$$\sigma\mathrm{D}^2\psi + \frac{1}{r^2}\left\{\frac{\partial\Psi_s}{\partial r}\frac{\partial}{\partial\zeta} - \frac{\partial\Psi_s}{\partial\zeta}\frac{\partial}{\partial r} + \frac{2\zeta}{1-\zeta^2}\frac{\partial\Psi_s}{\partial r} + \frac{2}{r}\frac{\partial\Psi_s}{\partial\zeta}\right\}\mathrm{D}^2\psi$$
$$+ \frac{1}{r^2}\left\{\frac{\partial\psi}{\partial r}\frac{\partial}{\partial\zeta} - \frac{\partial\psi}{\partial\zeta}\frac{\partial}{\partial r} + \frac{2\zeta}{1-\zeta^2}\frac{\partial\psi}{\partial r} + \frac{2}{r}\frac{\partial\psi}{\partial\zeta}\right\}\mathrm{D}^2\Psi_s - \frac{2}{Re}\mathrm{D}^4\psi = 0, \tag{3.6}$$

subject to the boundary conditions

$$\psi(1,\zeta)=0, \quad \frac{\partial\psi(1,\zeta)}{\partial r}=0, \tag{3.7a,b}$$

$$\lim_{r\to\infty}\psi(r,\zeta)\to 0, \tag{3.8}$$

and the symmetry conditions

$$\psi(r,1)=0, \quad \psi(r,-1)=0. \tag{3.9a,b}$$

We have solved this linear eigenvalue problem for the axisymmetric disturbances by a numerical technique akin to that used in the base-flow calculation, in which the radial coordinate is transformed to the finite domain $-1\leqslant z\leqslant 1$ according to

$$r=\exp(\tfrac{1}{2}a(z+1)). \tag{3.10}$$

Equations (3.6), (3.7) and (3.9) are straightforwardly transformed into the finite domain. If the far-field boundary condition (3.8) is satisfied at $z=1$ (i.e. at finite r), then it is of the 'hard' type discussed by Fornberg (1980). The fourth-order stream-function formulation for the axisymmetric disturbances requires two far-field conditions on the function $\tilde{\psi}(z,\zeta)=\psi(r,\zeta)$, which we take to be the 'soft' conditions

$$\frac{\partial\tilde{\psi}(z,\zeta)}{\partial z}=0, \quad \frac{\partial^3\tilde{\psi}(z,\zeta)}{\partial z^2}=0, \tag{3.11a,b}$$

applied at $z=1$.

As in the calculation of the base flow, we have followed the approach of Zebib (1987) and expanded the highest z-derivative of $\tilde{\psi}$ in terms of complete sets of functions in the z- and ζ-coordinates

$$\frac{\partial^4\tilde{\psi}(z,\zeta)}{\partial z^4}=\sum_{i=1}^{\infty}W_i(\zeta)\frac{\mathrm{d}^4H_i(z)}{\mathrm{d}z^4}, \tag{3.12}$$

where the radial functions are expanded in terms of Chebyshev polynomials

$$\frac{\mathrm{d}^4H_i(z)}{\mathrm{d}z^4}=\sum_{j=0}^{\infty}A_{ij}T_j(z), \tag{3.13a}$$

and the angular functions

$$W_i(\zeta)=\int_{\zeta}^{1}P_i(\zeta')\,\mathrm{d}\zeta', \tag{3.13b}$$

individually satisfy the symmetry conditions, where $P_i(\zeta)$ is the ith Legendre polynomial.

We next truncate (3.12) and (3.13a) to I and $J+1$ terms in the polar and radial directions, respectively, and integrate with respect to z to obtain expressions for ψ and its first three z-derivatives. The constants of integration are chosen so that each radial function $H_i(z)$ satisfies all of the boundary conditions. The result is

$$\frac{\mathrm{d}^nH_i}{\mathrm{d}z^n}=\sum_{j=0}^{J}A_{ij}\sum_{q=0}^{J+4-n}G_{qj}^{(n)}T_q(z) \quad (0\leqslant n\leqslant 3), \tag{3.14}$$

where the coefficients $G_{qj}^{(n)}$ are given in the Appendix.

That the boundary and symmetry conditions are automatically satisfied by any linear combination of the functions in (3.12) allows further consideration to be restricted to the partial differential equation (3.6). Rewriting this as

$$\sigma\mathrm{D}^2\tilde{\psi}+L(\tilde{\psi})-\frac{2}{Re}\mathrm{D}^4\tilde{\psi}=0, \tag{3.15}$$

Re	$I = J = 10$	$I = J = 14$	$I = J = 18$
50	$-9.638 \times 10^{-4} \pm 9.688 \times 10^{-3}$ i	$-8.861 \times 10^{-4} \pm 9.749 \times 10^{-3}$ i	$-9.062 \times 10^{-4} \pm 9.740 \times 10^{-3}$ i
130	$-6.781 \times 10^{-4} \pm 9.525 \times 10^{-3}$ i	$-6.002 \times 10^{-4} \pm 9.670 \times 10^{-3}$ i	$-6.301 \times 10^{-4} \pm 9.689 \times 10^{-3}$ i
160	$-5.355 \times 10^{-4} \pm 9.524 \times 10^{-3}$ i	$-5.127 \times 10^{-4} \pm 9.671 \times 10^{-3}$ i	$-5.311 \times 10^{-4} \pm 9.691 \times 10^{-3}$ i
170	$-4.804 \times 10^{-4} \pm 9.533 \times 10^{-3}$ i	$-4.817 \times 10^{-4} \pm 9.675 \times 10^{-3}$ i	$-4.921 \times 10^{-4} \pm 9.695 \times 10^{-3}$ i
180	$-4.139 \times 10^{-4} \pm 9.564 \times 10^{-3}$ i	$-4.510 \times 10^{-4} \pm 9.677 \times 10^{-3}$ i	$-4.612 \times 10^{-4} \pm 9.698 \times 10^{-3}$ i
190	$-3.585 \times 10^{-4} \pm 9.615 \times 10^{-3}$ i	$-4.175 \times 10^{-4} \pm 9.681 \times 10^{-3}$ i	$-4.308 \times 10^{-4} \pm 9.701 \times 10^{-3}$ i

TABLE 1. Least stable temporal eigenvalue for $m = 0$ with $r_\infty = 148.4$.

we formulate a weighted residuals procedure whereby the residual of the discretized (3.15) is made orthogonal to the trial functions according to

$$\int_1^{e^a} \int_0^{\pi} \left[\sigma \mathrm{D}^2 \tilde{\psi} + L(\tilde{\psi}) - \frac{2}{\mathrm{Re}} \mathrm{D}^4 \tilde{\psi} \right] V_i(\theta) S_j(r) r^k \sin\theta \, \mathrm{d}\theta \, \mathrm{d}r = 0,$$

for $1 \leqslant i \leqslant I$ and $0 \leqslant j \leqslant J$, where

$$V_i(\theta) = W_i(\zeta), \quad S_j(r) = \sum_{q=0}^{J+4} G_{qj}^{(0)} T_q(z).$$

Thus, the problem is reduced to a $I(J+1) \times I(J+1)$ matrix eigenvalue problem

$$\boldsymbol{A}\boldsymbol{x} = \sigma \boldsymbol{C}\boldsymbol{x}, \tag{3.16}$$

which is solved using standard numerical software (Garbow *et al.* 1977). That (3.16) is non-singular and has no spurious eigenvalues (Gottlieb & Orszag 1977) is guaranteed by satisfying the boundary and symmetry conditions (which do not involve σ) on a term-by-term basis in (3.13*a*, *b*) rather than by inclusion in (3.16) (Zebib 1987).

Table 1 shows the least stable temporal eigenvalue of (3.16) for $(I, J) = (10, 10)$, (14, 14) and (18, 18), computed with $a = 5$, corresponding to a computational domain consisting of a spherical annulus with radii 1 and $r_\infty \equiv \mathrm{e}^a = 148.4$. Additional calculations show that when the base-flow and disturbance equations are solved on a smaller domain ($r_\infty = 90.0$), the computed temporal eigenvalues (with $I = J = 14$) differ by 4.5 and 3.3% at $Re = 130$ and 190, respectively. The results clearly indicate that for $Re \leqslant 190$, all of the eigenvalues σ of the discretization are in the left half-plane. We therefore conclude that for $Re \leqslant 190$, the flow is stable with respect to axisymmetric disturbances.

The stability of the flow with respect to axisymmetric disturbances at higher Re was not investigated because of the discovery (see §3.2) of an instability with respect to non-axisymmetric disturbances (with azimuthal wavenumber $m = 1$) at $Re = 175.1$.

3.2. *Non-axisymmetric* ($m \neq 0$) *disturbances*

Linear analysis of the stability of non-axisymmetric disturbances (i.e. $m \neq 0$) proceeds from the Fourier decompositions (3.1*a*, *b*). Due to the axisymmetry of the base flow and the linearity of the disturbance equations, the individual Fourier modes are uncoupled and can be investigated separately. Because the disturbance variables $\boldsymbol{u}'$ and p' must be real, we require that $\boldsymbol{u}_{-m} = \boldsymbol{u}_m^*$ and $p_{-m} = p_m^*$, where * denotes a complex conjugate. As the case $m = 0$ has been treated in §3.1, attention will be restricted to $m \geqslant 1$.

We have found it convenient to use the primitive variables form of (2.1), (2.2) in this part of the analysis. The mth Fourier component of the disturbance is then governed by

$$\nabla \cdot \boldsymbol{u}_m = 0, \tag{3.17}$$

$$\frac{\partial \boldsymbol{u}_m}{\partial t} + (\boldsymbol{u}_m \cdot \nabla)\, \boldsymbol{U}_s + (\boldsymbol{U}_s \cdot \nabla)\, \boldsymbol{u}_m = -\nabla p_m + \frac{2}{Re} \nabla^2 \boldsymbol{u}_m, \tag{3.18}$$

with the no-slip boundary condition

$$\boldsymbol{u}_m(1, \theta, \phi, t) = 0. \tag{3.19}$$

We then make the change of variables $\zeta = \cos\theta$ and eliminate the pressure and azimuthal velocity component as follows. We first note that $\partial \boldsymbol{u}_m / \partial \phi = im\boldsymbol{u}_m$ and use (3.17) to eliminate $u_{m\phi}$ from (3.17), (3.18). In the same manner, we can solve the azimuthal momentum equation for p'_m, and hence eliminate p_m.

As with axisymmetric disturbances, we consider modal solutions of the form

$$u'_{mr}(r, \zeta, t) = \mathrm{e}^{\sigma t}\, \hat{u}_{mr}(r, \zeta), \tag{3.20a}$$

$$u'_{m\zeta}(r, \zeta, t) = \mathrm{e}^{\sigma t}\, \hat{u}_{m\zeta}(r, \zeta), \tag{3.20b}$$

leading to two coupled equations in r and ζ which constitute an eigenvalue problem for σ.

The final result is a pair of partial differential equations for the r- and ζ-components of the velocity of the form

$$\begin{aligned}
&\sigma\left[m^2 \hat{u}_{mr} + \sin^2\theta \frac{\partial}{\partial r}(r h_m)\right] \\
&\quad + m^2\left[\frac{\partial}{\partial r}(U_{sr}\, \hat{u}_{mr}) - \frac{\sin\theta}{r}\left(\frac{\partial U_{sr}}{\partial \zeta}\hat{u}_{m\zeta} + U_{s\zeta}\frac{\partial \hat{u}_{mr}}{\partial \zeta}\right) - \frac{2}{r} U_{s\zeta}\hat{u}_{m\zeta}\right] \\
&\quad + \sin^2\theta \frac{\partial}{\partial r}\left[r U_{sr}\frac{\partial h_m}{\partial r} - U_{s\zeta}\frac{\partial}{\partial \zeta}(h_m \sin\theta) + U_{sr} h_m + h_m U_{s\zeta}\cot\theta\right] \\
&\quad + \frac{2}{Re}\left\{\frac{m^2}{r^2}\left[-\frac{\partial}{\partial r}\left(r^2\frac{\partial \hat{u}_{mr}}{\partial r}\right) - \frac{\partial}{\partial \zeta}\left(\sin^2\theta\frac{\partial \hat{u}_{mr}}{\partial \zeta}\right) + 2\hat{u}_{mr} + \frac{m^2}{\sin^2\theta}\hat{u}_{mr}\right]\right. \\
&\quad - \sin\theta\frac{\partial}{\partial r}\left[\frac{\sin\theta}{r}\frac{\partial}{\partial r}\left(r^2\frac{\partial h_m}{\partial r}\right) + \frac{1}{r}\frac{\partial}{\partial \zeta}\left(\sin^2\theta\frac{\partial}{\partial \zeta}(h_m \sin\theta)\right)\right] \\
&\quad \left. + (1+m^2)\frac{\partial}{\partial r}\left(\frac{h_m}{r}\right) + 2m^2\left[\cot\theta\frac{\partial}{\partial r}\left(\frac{\hat{u}_{m\zeta}}{r}\right) - \frac{3}{r^2}\hat{u}_{mr}\right]\right\} = 0,
\end{aligned} \tag{3.21a}$$

$$\begin{aligned}
&\sigma\left[m^2 \hat{u}_{m\zeta} - \sin\theta\frac{\partial}{\partial \zeta}(h_m \sin^2\theta)\right] \\
&\quad + m^2\left[\hat{u}_{mr}\left(\frac{\partial}{\partial r} + \frac{1}{r}\right)U_{s\zeta} + U_{sr}\left(\frac{\partial}{\partial r} + \frac{1}{r}\right)\hat{u}_{m\zeta} - \frac{\sin\theta}{r}\frac{\partial}{\partial \zeta}(U_{s\zeta}\hat{u}_{m\zeta})\right] \\
&\quad - \sin\theta\frac{\partial}{\partial \zeta}\left[\sin^2\theta\left(U_{sr}\frac{\partial h_m}{\partial r} - \frac{U_{s\zeta}}{r}\frac{\partial}{\partial \zeta}(h_m \sin\theta) + \frac{U_{sr}}{r}h_m + \frac{U_{s\zeta}}{r}h_m\cot\theta\right)\right] \\
&\quad + \frac{2}{Re}\left\{\frac{m^2}{r^2}\left[-\frac{\partial}{\partial r}\left(r^2\frac{\partial \hat{u}_{m\zeta}}{\partial r}\right) - \frac{\partial}{\partial \zeta}\left(\sin^2\theta\frac{\partial \hat{u}_{m\zeta}}{\partial \zeta}\right) + \frac{1+m^2}{\sin^2\theta}\hat{u}_{m\zeta} - 2\sin\theta\frac{\partial}{\partial \zeta}(\hat{u}_{m\zeta}\cot\theta)\right]\right.
\end{aligned}$$

$$+\frac{\sin\theta}{r^2}\frac{\partial}{\partial\zeta}\left[\sin^2\theta\frac{\partial}{\partial r}\left(r^2\frac{\partial h_m}{\partial r}\right)+\sin\theta\frac{\partial}{\partial\zeta}\left(\sin^2\theta\frac{\partial}{\partial\zeta}(h_m\sin\theta)\right)\right]$$

$$-\frac{1+m^2}{r^2}\sin\theta\frac{\partial h_m}{\partial\zeta}+\frac{2m^2}{r^2}h_m\cot\theta\Big\}=0, \tag{3.21b}$$

where

$$h_m=\frac{\partial}{\partial\zeta}(\hat{u}_{m\zeta}\sin\theta)-\frac{1}{r}\frac{\partial}{\partial r}(r^2\hat{u}_{mr}).$$

Here, the velocity components must satisfy the boundary conditions

$$\hat{u}_{mr}(1,\zeta)=0,\quad \hat{u}_{m\zeta}(1,\zeta)=0, \tag{3.22a,b}$$

on the sphere. Following Batchelor & Gill (1962), the disturbance must also satisfy the kinematic conditions

$$\hat{u}_{mr}(r,\pm1)=0\quad(m\geqslant1), \tag{3.22c}$$

$$\hat{u}_{1\zeta}(r,\pm1)\text{ bounded}, \tag{3.22d}$$

$$\hat{u}_{m\zeta}(r,\pm1)=0\quad(m>1), \tag{3.22e}$$

on the coordinate axes $\zeta=\pm1$.

As in §3.1, the numerical treatment begins with the transformation (3.10) of the radial variable. The transformed counterparts of (3.21 a,b) contain fourth derivatives of $\tilde{u}_{mz}(z,\zeta)=\hat{u}_{mr}(r,\zeta)$ and third derivatives of $\tilde{u}_{m\zeta}(z,\zeta)=\hat{u}_{m\zeta}(r,\zeta)$ with respect to z. The boundary conditions satisfied by $\tilde{u}_{mz}$ and $\tilde{u}_{m\zeta}$ are then

$$\tilde{u}_{mz}(-1,\zeta)=0,\quad \frac{\partial\tilde{u}_{mz}(-1,\zeta)}{\partial z}=0, \tag{3.23a,b}$$

and

$$\tilde{u}_{m\zeta}(-1,\zeta)=0, \tag{3.23c}$$

at the surface of the sphere. Here (3.23 a,c) follow directly from (3.22 a,b), whereas (3.23 b) is a direct consequence of the continuity equation.

The z- and ζ-components of the velocity are then required to satisfy two far-field boundary conditions at $z=1$. As in the calculation of the base flow and the investigation of axisymmetric disturbances, there is a degree of choice available in the selection of these far-field conditions. We have chosen to require that each of the disturbance velocity components satisfy a 'hard' and a 'soft' boundary condition at $z=1$. These are

$$\tilde{u}_{mz}(1,\zeta)=0,\quad \tilde{u}_{m\zeta}(1,\zeta)=0, \tag{3.23d,e}$$

and

$$\frac{\partial\tilde{u}_{mz}(1,\zeta)}{\partial z}=0,\quad \frac{\partial\tilde{u}_{m\zeta}(1,\zeta)}{\partial z}=0, \tag{3.23f,g}$$

where the hard conditions (3.23 d,e) ensure that the disturbance inflow is axisymmetric on the outer boundary of the computational domain.

We now consider solution of an eigenvalue problem consisting of the partial differential equations (3.21 a,b) and the boundary and kinematic conditions (3.22), (3.23). This time, we expand the disturbance quantities directly in terms of a complete set of functions. (A similar procedure had earlier been attempted for the base-flow calculation, but was abandoned owing to slow convergence of the Newton

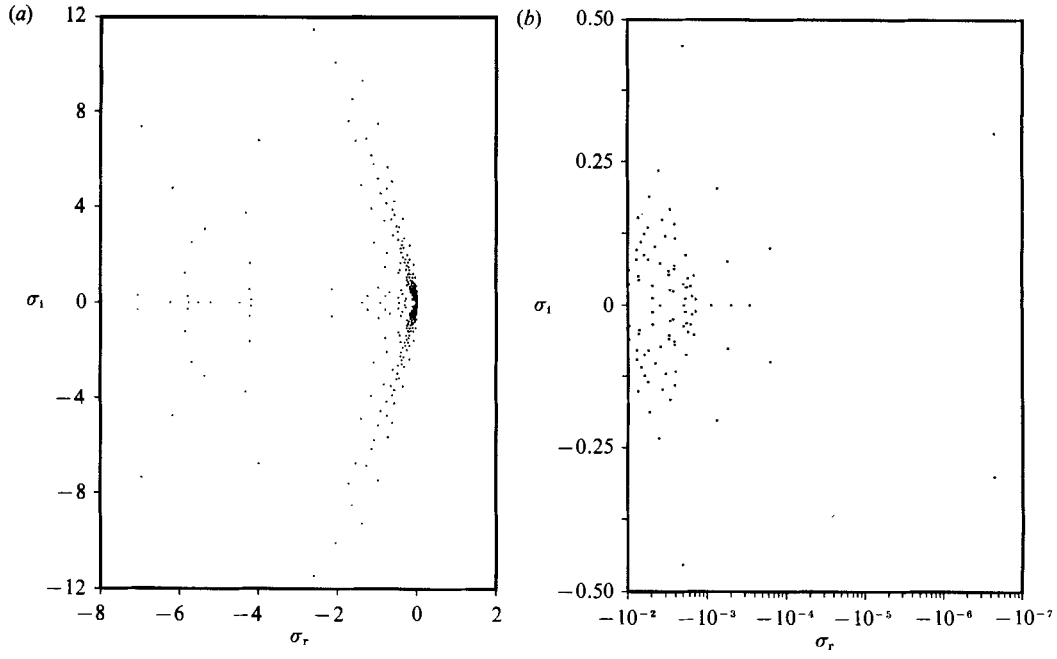

FIGURE 1. Distribution of the temporal eigenvalues for $m = 1$ and $Re = 175$, with $I = J = 14$, $r_\infty = 148.4$. (*a*) All of the temporal eigenvalues. (*b*) Detail showing the least stable eigenvalues.

iteration used to solve the nonlinear algebraic equation system.) The expansion for $m = 1$

$$\tilde{u}_{1z}(z,\zeta) = \sum_{i=1}^{I} W_i(\zeta) \sum_{j=0}^{J} B_{ij}\, e^{-\frac{1}{2}a(z+1)}(z^2-1)^2 z^j, \tag{3.24a}$$

$$\tilde{u}_{1\zeta}(z,\zeta) = \sum_{i=0}^{I} P_i(\zeta) \sum_{j=0}^{J} E_{ij}\, e^{-\frac{1}{2}a(z+1)}(z^2-1)(z-1) z^j, \tag{3.24b}$$

differs from the general case on account of the kinematic condition (3.22*e*). We denote by $R_1(z,\zeta)$ and $\Theta_1(z,\zeta)$ the residuals that result when the expansions (3.24*a*, *b*) are substituted into the differential equations (3.21*a*) and (3.21*b*), respectively. We then make these residuals orthogonal to the trial functions according to

$$\int_{-1}^{1}\int_{-1}^{1} R_1(z,\zeta)\, W_i(\zeta)(z^2-1)^2 z^j \,d\zeta\, dz = 0 \quad (1 \leqslant i \leqslant I, \quad 0 \leqslant j \leqslant J), \tag{3.25a}$$

$$\int_{-1}^{1}\int_{-1}^{1} \Theta_1(z,\zeta)\, P_i(\zeta)(z^2-1)(z-1) z^j \,d\zeta\, dz = 0 \quad (0 \leqslant i \leqslant I, \quad 0 \leqslant j \leqslant J). \tag{3.25b}$$

These linear equations constitute a matrix eigenvalue problem of the form (3.16), where $\boldsymbol{C}$ is again non-singular. In the non-axisymmetric case, the order of the eigenvalue problem is $(J+1)(2I+1)$. Again, the eigenproblem is solved using standard EISPACK software. No spurious eigenvalues were found. For Re near Re_1, computation of the base flow (with $K = L = 28$) requires four Newton iterations, amounting to about 16 min of CRAY X-MP/48 time. Determination of the stability of the base flow (with $I = J = 14$) requires an additional 20 min on the same machine.

Table 2 shows, for $m = 1$ and $160 \leqslant Re \leqslant 190$, the temporal eigenvalue σ having the largest real part, for $r_\infty = 148.4$ and $(I, J) = (12, 12)$, $(14, 14)$, $(16, 16)$ and $(14, 16)$.

Re	$I = J = 12$	$I = J = 14$	$I = 14, J = 16$	$I = J = 16$
160	$-2.153 \times 10^{-4} \pm 0.0986$ i	$-1.985 \times 10^{-4} \pm 0.0996$ i	$-2.075 \times 10^{-4} \pm 0.0995$ i	$-2.095 \times 10^{-4} \pm 0.0996$ i
170	$-6.428 \times 10^{-5} \pm 0.3111$ i	$-5.316 \times 10^{-5} \pm 0.3001$ i	$-5.773 \times 10^{-5} \pm 0.3012$ i	$-5.937 \times 10^{-5} \pm 0.3004$ i
175	$-3.041 \times 10^{-6} \pm 0.3113$ i	$-2.261 \times 10^{-7} \pm 0.3001$ i	$-1.002 \times 10^{-6} \pm 0.3013$ i	$-1.052 \times 10^{-6} \pm 0.3004$ i
175.2	$+1.425 \times 10^{-6} \pm 0.3115$ i	$+4.458 \times 10^{-7} \pm 0.3000$ i	$+1.486 \times 10^{-6} \pm 0.3010$ i	$+1.512 \times 10^{-6} \pm 0.3002$ i
180	$+8.349 \times 10^{-5} \pm 0.3115$ i	$+9.453 \times 10^{-5} \pm 0.3000$ i	$+9.035 \times 10^{-5} \pm 0.3010$ i	$+8.912 \times 10^{-5} \pm 0.3002$ i
190	$+2.134 \times 10^{-4} \pm 0.3115$ i	$+2.012 \times 10^{-4} \pm 0.3000$ i	$+2.102 \times 10^{-4} \pm 0.3010$ i	$+2.105 \times 10^{-4} \pm 0.3002$ i

TABLE 2. Least stable temporal eigenvalue for $m = 1$ with $r_\infty = 148.4$.

$I = J$	$K = L = 28$	$K = 28, L = 34$	$K = 40, L = 28$
12	$-3.041 \times 10^{-6} \pm 0.3113$ i	$-3.050 \times 10^{-6} \pm 0.3110$ i	$-3.048 \times 10^{-6} \pm 0.3114$ i
14	$-2.261 \times 10^{-7} \pm 0.3001$ i	$-2.972 \times 10^{-7} \pm 0.3005$ i	$-2.756 \times 10^{-7} \pm 0.3002$ i
16	$-1.052 \times 10^{-6} \pm 0.3004$ i	$-1.143 \times 10^{-6} \pm 0.3000$ i	$-1.095 \times 10^{-6} \pm 0.3003$ i

TABLE 3. Least stable eigenvalue for $m = 1$, $Re = 175$ with $r_\infty = 148.4$.

Re	
160	$-8.116 \times 10^{-4} \pm 0.0$ i
170	$-7.907 \times 10^{-4} \pm 0.0$ i
180	$-7.687 \times 10^{-4} \pm 0.0$ i
190	$-7.439 \times 10^{-4} \pm 0.0$ i

TABLE 4. Least stable temporal eigenvalue for $m = 2$ with $r_\infty = 148.4$, $I = J = 14$.

(We have considered $I = J$ and $I \neq J$ in order to examine the possible dependence of Re_1 and the disturbance eigenfunction on the truncation scheme employed (Steen & Aidun 1988).) As in the $m = 0$ case, calculations using $r_\infty = 90.0$ gave least stable (most unstable) temporal eigenvalues differing only modestly from the results for $r_\infty = 148.4$ at $Re = 130$ and 190 (6.5 and 9.5%, respectively).

The results indicate that disturbances with azimuthal wavenumber $m = 1$ become unstable at $Re \approx 175.1$. The imaginary part of the neutral eigenvalue is $\Omega \approx 0.300$, corresponding to a Hopf bifurcation, and indicates that the onset of instability occurs via oscillatory disturbances. If the frequency is non-dimensionalized in the same way as a Strouhal number (based on sphere diameter), we obtain $St_1 = \Omega/\pi = 0.0955$. The computed values of Re_1 and St_1 are in excellent agreement with experiment, as discussed in §4.

Figure 1 shows the distribution of the temporal eigenvalues at $Re = 175$ with $I = J = 14$ and $r_\infty = 148.4$. From figure 1(*a*), we note that the eigenvalues are clustered along a curve which passes near to the origin of the σ-plane. Figure 1(*b*) shows that although a pair of eigenvalues with $\mathrm{Im}(\sigma) = 0.300$ is the least stable at $Re = 175$, there are many other eigenvalues having real parts which are only slightly negative.

Table 3 shows that the number of trial functions employed in the base-flow calculation ($K = L = 28$) is sufficient.

For $m > 1$, the linear-disturbance equations are still (3.21*a*, *b*) and (3.22*c*), (3.23), with (3.22*d*) replaced by (3.22*e*). We employ the expansions

$$\tilde{u}_{mz}(z, \zeta) = \sum_{i=1}^{I} W_i(\zeta) \sum_{j=0}^{J} F_{ij}\, \mathrm{e}^{-a(z+1)}(z^2-1)^2 z^j,$$

$$\tilde{u}_{m\zeta}(z, \zeta) = \sum_{i=1}^{I} W_i(\zeta) \sum_{j=0}^{J} X_{ij}\, \mathrm{e}^{-a(z+1)}(z^2-1)(z-1) z^j.$$

As before, these expressions are substituted into (3.21*a*, *b*), and the residuals are made orthogonal to the trial functions. The resulting set of $2I(J+1)$ homogeneous linear algebraic equations again constitutes an eigenvalue problem of the form (3.16), which is solved as before.

The results shown in table 4 clearly indicate that the flow is stable for disturbances with $m = 2$ for $Re < Re_1$. Table 5 suggests that the flow becomes increasingly stable with respect to disturbances having larger azimuthal wavenumbers, at least near Re_1.

m	
2	$-7.775\times10^{-4}\pm0.0\,\mathrm{i}$
3	$-1.193\times10^{-3}\pm2.348\times10^{-2}\,\mathrm{i}$
4	$-1.285\times10^{-3}\pm2.377\times10^{-2}\,\mathrm{i}$
5	$-1.302\times10^{-3}\pm2.375\times10^{-2}\,\mathrm{i}$

TABLE 5. Least stable temporal eigenvalue for $Re = 175$, with $r_\infty = 148.4$, $I = J = 14$.

Finally, we remark on the interpretation of our analysis. For either axisymmetric or non-axisymmetric disturbances, the problem reduces to one of deciding whether the spectra of certain linear partial differential operators lie entirely in the left half-plane. We have approximated the linear operators by finite-dimensional matrices, the eigenvalues of which are taken to approximate those of the corresponding differential operators. This approach leaves in some doubt the status of the continuous spectrum of the original operator. Although we cannot prove that the continuous spectra (if in fact they exist) lie entirely in the left half-plane for all combinations of Re and m investigated, there is every reason (based on the reasonable agreement with experiment and the distribution of eigenvalues shown in figure 1) to believe that the present results are in fact not corrupted by the discretization.

3.3. *Structure of the $m = 1$ eigenfunction*

In order to better understand the three-dimensional character of the non-axisymmetric disturbance that becomes unstable at Re_1, we have examined an approximation to the oscillating wake. In particular, we have considered a composite flow consisting of the axisymmetric base flow to which is added some multiple of the eigenfunction of the linear stability problem, i.e.

$$\boldsymbol{u}_c(r,\theta,\phi,t) = \boldsymbol{U}_s(r,\theta) + \mathrm{Re}\{\boldsymbol{u}_1(r,\theta,\phi,t)\}, \tag{3.26}$$

with the amount of the linear eigenfunction added to the base flow chosen so that the maximum speed of the disturbance flow ($|\boldsymbol{u}_1|$) is 0.0174, where the characteristic velocity of the base flow is unity, corresponding to the uniform flow. Although (3.26) is no longer a numerical solution of the full Navier–Stokes equations, it should give a good qualitative picture of the actual flow just above Re_1 if instability sets in via oscillations of small amplitude (infinitesimal amplitude at the bifurcation point).

For this composite flow, we have selected $Re = 175.1$, and computed the pathline for a fluid particle having an initial position $r = 1.2$ and $\theta = 30°$. This point lies within the recirculating flow region for the base flow with $Re = 175.1$. Figure 2 shows two perspective views of the pathlines at a sequence of dimensionless times. We observe that the pathline resembles a trajectory on a torus having a highly non-circular, slightly ϕ-dependent cross-section. In fact, the perimeter of the cross-section of the torus closely approximates a pathline (in a constant ϕ-plane) of the steady axisymmetric base flow. The helical nature of the disturbance is clearly evident. At larger Re (corresponding to a larger azimuthal velocity component), the pathlines will be less tightly wound. For either the composite flow (3.26) or a time-periodic solution of the nonlinear equations (2.1)–(2.3), we can easily show that the particle trajectories will not be temporally periodic unless Re is chosen so that the pathline winds around the toroidal cross-section an integral number of times during a 2π change in ϕ.

The $m = 1$ eigenfunction can also be characterized in terms of the disturbance

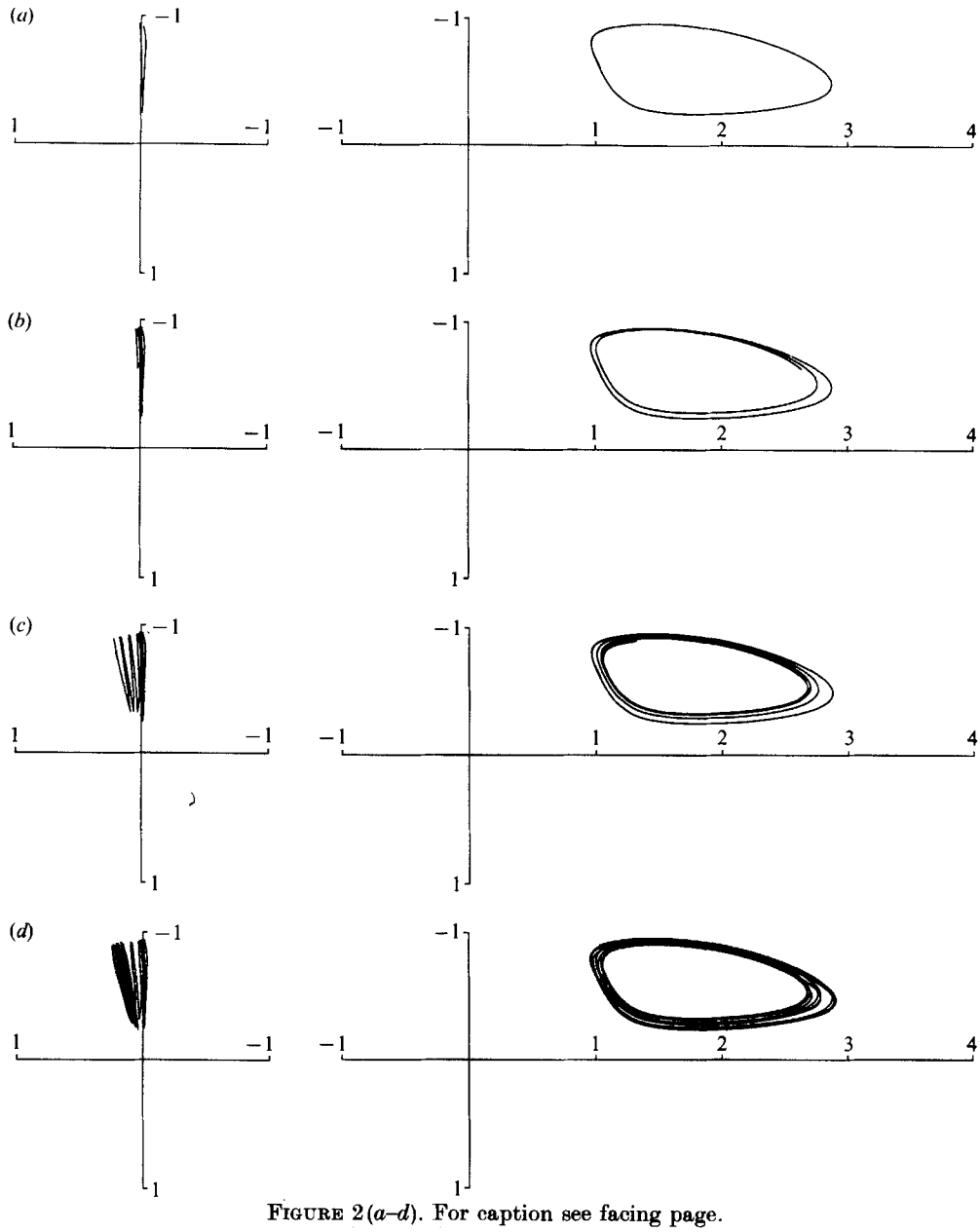

FIGURE 2(a–d). For caption see facing page.

vorticity field. Figures 3(a)–(c) show the r- and θ-dependence of the azimuthal, polar and radial components of the disturbance vorticity, with the real and imaginary parts in the upper and lower halves, respectively, of each figure. We note that the disturbance is strongest near the equator of the sphere, upstream of the separation point, which is located at $\theta = 63.4°$ for $Re = 175$. In each of the six cases (real and imaginary parts of the three vorticity components), inspection of the entire field out to $r = 148.4$ revealed no other vorticity contours with level equal to or exceeding the contours shown. It is thus clear that although the disturbance manifests itself as a

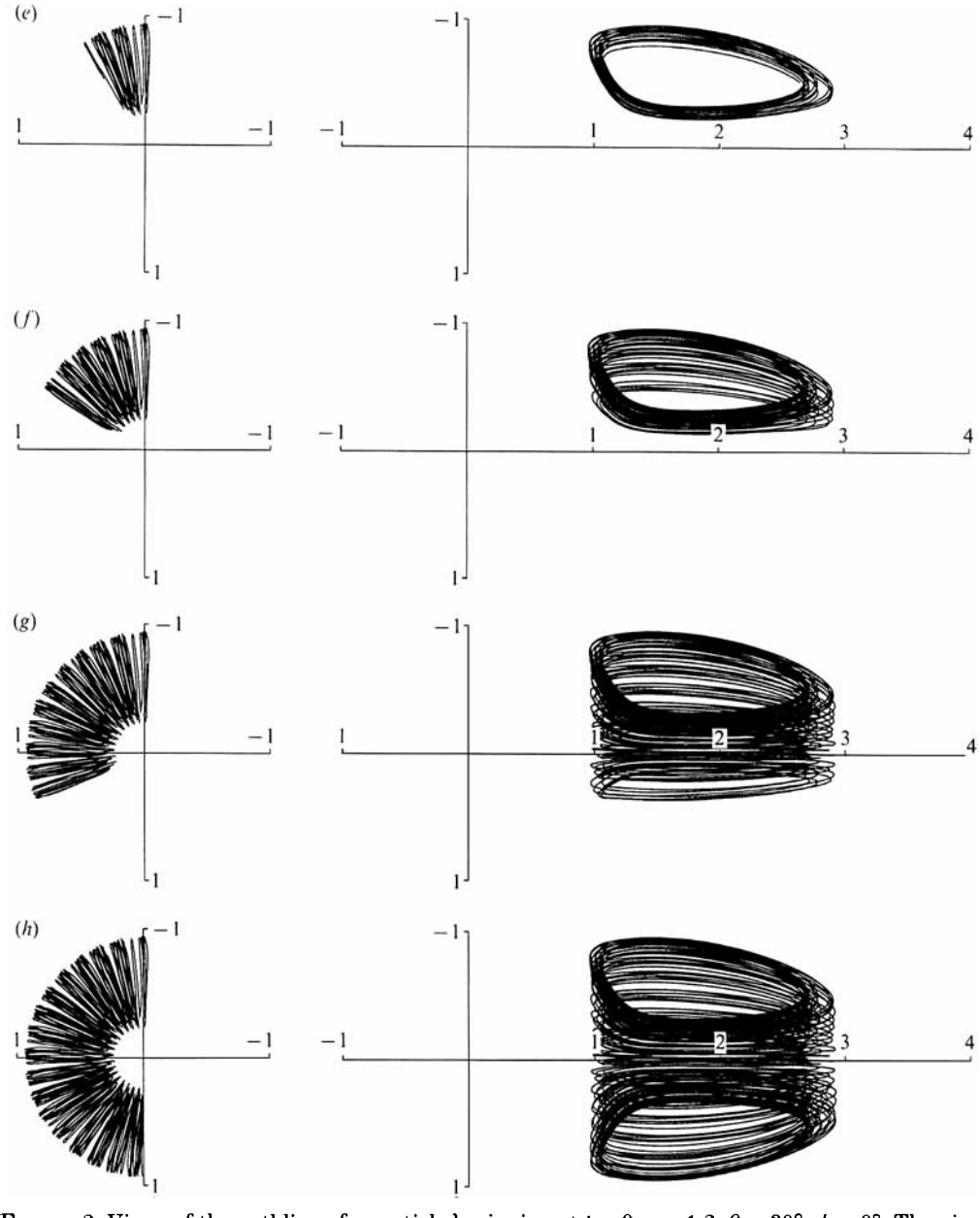

FIGURE 2. Views of the pathline of a particle beginning at $t = 0$, $r = 1.2$, $\theta = 30°$, $\phi = 0°$. The views on the right are from a point two sphere radii downstream of the sphere centre (located at the intersection of the two axes shown), 100 sphere radii from a plane passing through the sphere centre, and inclined 270° with respect to the $\sin\phi = 0$ plane in which the particle's initial condition lies. The views on the left are from a point 100 sphere radii upstream of the sphere centre (again at the intersection of the axes shown), located on the base flow's symmetry axis. The pathline is shown at $t = 30$, 60, 120, 240, 480, 960, 1920, 3084.

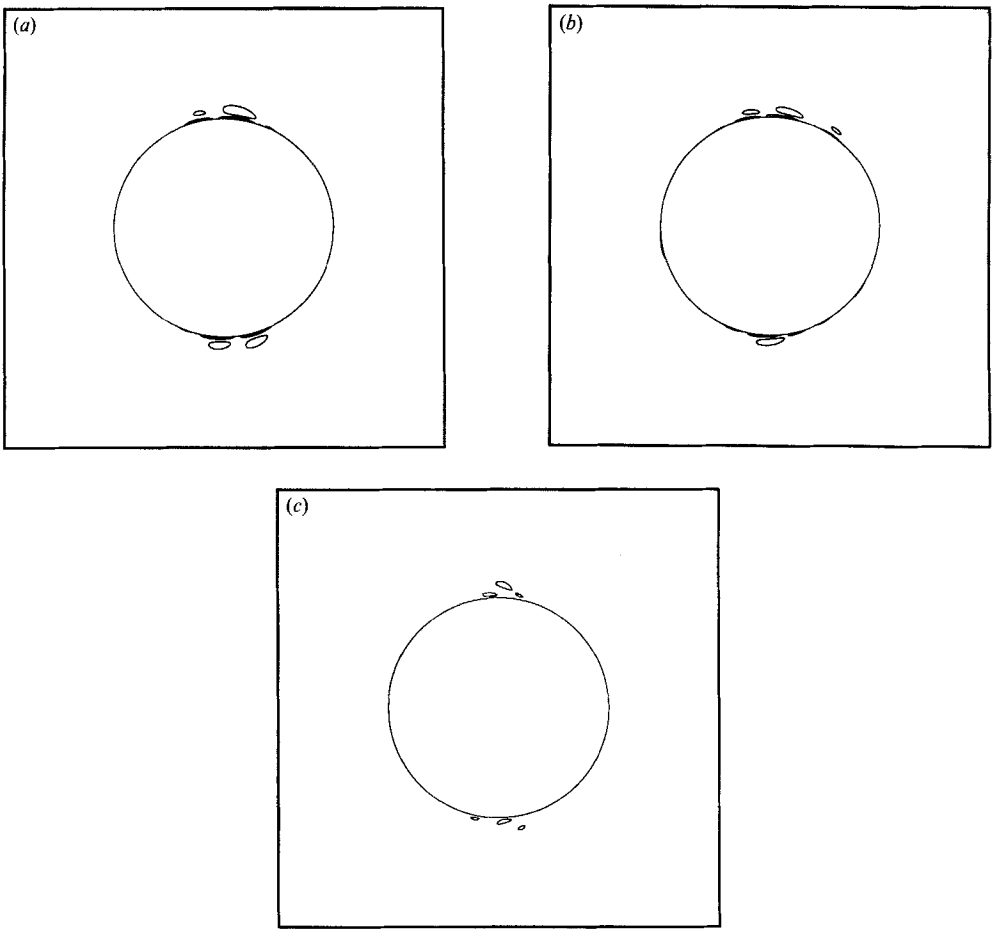

FIGURE 3. $r-\theta$ dependence of the real and imaginary parts of the three vorticity components. (a) ω_ϕ; (b) ω_θ; (c) ω_r. The upper and lower halves of each figure depict the real and imaginary parts, respectively, of the appropriate vorticity component.

helical motion in the wake, its origin is in the instability of the boundary-layer flow on the sphere.

4. Comparison to experiment

In this section, we compare our computational results to a number of previous experiments. As discussed below, the experimental determination of Re_1 is complicated by the fact that the wake oscillations have a very low frequency. In view of this problem, we believe that the comparisons presented here are very good.

Möller (1938) towed spheres equipped with dye ports vertically through water in tanks of square cross-section. He found that the flow was steady below $Re = 170$, and that at $Re = 200$, the wake oscillated with a very low frequency. The ratio of tank width to sphere diameter was 8 at $Re = 170$ and 20 at $Re = 200$. In view of the rather large blockage factor, we consider the agreement between Möller's experiment and our calculation to be very good.

Taneda (1956) reported that when a 'Reynolds number of about 130 is reached,

however, the faint periodic pulsatile motion with a very long period occurs at the rear of the vortex-ring'. Taneda gave a possible explanation for his observation of unsteadiness at an Re below our computed Re_1 when he noted 'that a slight asymmetry of the flow pattern was caused by the presence of the support; namely the separation point just behind the support was moved slightly forward'. The fact that the spheres were suspended by a single vertical support (with the base flow being primarily in the horizontal direction) means that, perforce, the distorted base flow had a substantial $m = 1$ component, which is the azimuthal mode to which the axisymmetric flow is most unstable. Moreover, as shown in figure 3(*a–c*), the disturbance eigenfunction is concentrated at the equator, where Taneda's spheres were supported. In addition, Taneda's use of thin piano wires (with diameters of 0.3 mm and 0.5 mm and aspect ratios of 50 and 30, respectively) to support much larger spheres (diameters between 9.52 mm and 19.82 mm) may allow considerable coupling between disturbances in the flow and the rigid body motion of the spheres. It seems likely that Re_1 for a fixed (i.e. rigidly supported) sphere will be greater than or equal to the Re_1 for a sphere which is allowed to respond to flow disturbances, because the disturbances to which the latter sphere are subject are less constrained than those to which the former are subject.) Thus, the lack of rigidity of the support may also contribute to Taneda's observation of instability at a lower Re than predicted by us.

Goldburg & Florsheim (1966) observed that the wake behind a falling sphere lost its axisymmetry at $Re \approx 210$, although they did not detect the loss of steadiness until $Re = 270$. We consider our results to be in good agreement with these, given the low-frequency nature of the instability, which makes the discernment of unsteadiness difficult.

Toulcova & Podzimek (1968) dropped aluminium alloy spheres through various solutions of glycerol and water, and reported that the transition to unsteadiness occurred at $Re = 130$. In a later study with the same spheres, Zikmundova (1970) reported a transition to unsteadiness in the range $130 < Re < 150$. Since Re_1 for falling spheres should approach the fixed-sphere value when the sphere/fluid density ratio ($\beta = \rho_s/\rho_f$) in the freely falling case approaches infinity, we might expect our computed Re_1 to be significantly higher than that found in these experiments, for which $\beta = 2.18$. (Although neither the composition nor the density of the solutions was given, subsequent enquiry (J. Goodman, private communication, 1984) revealed that in all cases, the glycerol mass fraction was in excess of 0.99, allowing the density ratio to be accurately determined.)

Roos & Willmarth (1971) found that for a sphere towed through water and supported by a sting in the rear, a side force first became apparent at $Re \approx 290$, corresponding to a non-axisymmetric force exerted on the sphere by the flow. They also found that if a weighted sphere was supported by two fine threads, the onset of the side force occurred at $Re \approx 215$. Roos (1968) concluded that the presence of a sting in the near wake had the effect of 'tying down the tail of the wake bubble through the no-slip condition at the sting surface', and that this prevented oscillation of the wake under conditions where it would have otherwise been unstable (i.e. for $215 \leqslant Re \leqslant 290$). We think that our computed value of $Re_1 = 175.1$ is in good agreement with the value ($Re \approx 215$) of Roos & Willmarth (1971).

Nakamura (1976) observed the trajectories of falling spheres to be vertical for $Re < 190$, with meandering at higher Re. Since it can be shown that the trajectory of a freely falling sphere subject to disturbances containing an $m = 1$ azimuthal component cannot be vertical, the onset of meandering corresponds to the onset of

Authors	Liquid	Distance travelled (cm)	U_∞ (cm/s)	Sphere radius (cm)	Remarks	Computed f (Hz)
Möller	Water	120	0.286	2.975	Towed	0.00472
	Water	120	0.278	3.050	Towed	0.00449
Taneda	Water	100	0.86	0.991	Towed	0.0425
	Water	100	1.13	0.754	Towed	0.0735
Nakamura	Water	100	1.373	0.619	Falling	0.109
Goldburg & Florsheim	30% glycerol 70% water	120	10.0	0.286	Falling	1.29

TABLE 6. Wake oscillation frequencies for previous experimental work, computed using equation (3.25), for $Re = 175.1$.

an $m = 1$ instability. Thus, we consider our results to be in excellent agreement with Nakamura's flow-visualization experiments.

As for the frequency of the wake oscillations near the onset of instability, there is relatively little quantitative data with which our results can be compared. Probably the best data at low Re (below the onset of vortex shedding) is that of Roos (1968), who towed a sphere supported by a side-sting in a 9.6 m long tank, and found $St_1 \approx 0.087$. (This is an average of measurements at the six lowest Re, in the range $250 < Re < 450$, with all values lying between 0.084 and 0.095.) We consider this to be in excellent agreement with our computed value $St_1 = 0.0955$.

In connection with the observations of Möller (1938) and Taneda (1956) regarding the low-frequency nature of the wake oscillations, it is of interest to note that the dimensional frequency

$$f = \frac{\Omega \nu Re}{4\pi R_0^2}, \tag{4.1}$$

corresponding to $\Omega = 0.300$ is very low in most of the previous experimental work in which Re_1 was estimated. Table 6 shows the sphere radii, fluids and dimensional frequencies (calculated according to (4.1) with $Re = 175.1$) for previous experiments. The low frequencies undoubtedly contribute to the difficulty in observing the wake oscillations, especially at or near Re_1. (The experimental work of Stringham *et al.* (1969) is not included in table 3 because their measured viscosity data for aqueous glycerol solutions are in serious disagreement with accepted sources (Segur & Oberstar 1951). We cannot correct for this by interpolating from the data of Segur & Oberstar because it is not known whether the discrepancy is due to poor viscometry or the absorption of atmospheric water by the extremely hygroscopic glycerol. We have also not included the data of Toulcova & Podzimek (1968) because of uncertainty about the degree to which the velocity of the falling sphere had approached its terminal value.)

5. Discussion

The present work provides the first accurate calculation of the critical Reynolds number at which the non-parallel flow past a body of revolution becomes unstable. Our results for a sphere are in good agreement with previous experimental work, for both Re_1 as well as the frequency of the wake oscillations. The predicted instability mode ($m = 1$) is the same as that observed experimentally at higher Re.

Our results are also in good agreement with the theoretical prediction by

Monkewitz (1988*b*) of local absolute instability for a class of parallel axisymmetric wake profiles. His results are for the $m = 1$ azimuthal mode and are parameterized by a centreline reversed flow parameter (Λ) and a shape parameter. In view of the fact that both the degree of reversed flow on the centreline, as well as the wake shape, depend on downstream distance (owing to the non-parallel nature of the flow), we have not attempted a direct comparison of our results for the sphere to Monkewitz's theory. However, we do note that our computed value $Re_1 = 175.1$, lies in the range ($10^2 < Re < 10^3$) in which Monkewitz has predicted the occurrence of local absolute instability for two values of Λ.

Since our analysis is a linear one that finds the smallest Re at which infinitesimally small disturbances will grow, the possibility remains that disturbances of finite amplitude might lead to the onset of subcritical instability at smaller Re. That the onset of instability in the steady axisymmetric base flow probably occurs by a linear mechanism is suggested by the agreement with experiment. First, the computed value of Re_1 and the associated Strouhal number are in good agreement with previous experimental values. (In those cases where the agreement between computed and experimental values of Re_1 leaves something to be desired, differences between experiment and the ideal situation considered in our analysis are consistent with the magnitudes and signs of the discrepancies.) Moreover, the predicted azimuthal wavenumber ($m = 1$) is the same as that observed in experiments at higher Re.

Finally, we note that it would be interesting to determine whether the Hopf bifurcation which seems to lead to unsteady helical vortex shedding is a supercritical one, as appears to be the case for transition from a steady separated wake to the Kármán vortex street in two-dimensional flow past a circular cylinder. This question could be investigated by a weakly nonlinear analysis, or by introducing disturbances into a three-dimensional time-dependent numerical simulation.

The authors thank Professor P. A. Monkewitz for useful comments. They are grateful to the National Science Foundation for support of this work under NSF Grant MSM-8451157, and to the NSF San Diego Supercomputer Center, where much of the computing was done.

Appendix

We can integrate (3.13*a*) to get

$$\frac{\mathrm{d}^n H_i}{\mathrm{d}z^n} = \sum_{j=0}^{J} A_{ij} \sum_{q=0}^{J+4-n} f_{qj}^{(n)}\, T_q(z) + \sum_{p=1}^{4-n} Q_p^{(n)}\, T_{p-1}(z) \quad (0 \leqslant n \leqslant 3), \tag{A 1}$$

where $Q_1^{(3)} = Q_2^{(2)} = 4Q_3^{(1)} = 24Q_4^{(0)} = \alpha_1$, $Q_1^{(2)} = Q_2^{(1)} = 4Q_3^{(0)} = \alpha_2$, $Q_1^{(1)} = \alpha_3$, $Q_1^{(0)} = \alpha_4$, $Q_2^{(0)} = \alpha_1 - \frac{1}{8}\alpha_1$, all other values of $Q_p^{(n)}$ are zero, the coefficients $f_{qj}^{(n)}$ are given by Zebib (1984), and the α_i are determined from the boundary conditions. We can then rewrite (A 1) as (3.14), where

$$\begin{aligned}
G_{qj}^{(3)} &= f_{qj}^{(3)} - \eta_j^{(3)}\delta_{q0},\\
G_{qj}^{(2)} &= f_{qj}^{(2)} - \eta_j^{(3)}\delta_{q1} - \tfrac{1}{2}[\eta_j^{(1)} - \gamma_j^{(1)}]\,\delta_{q0},\\
G_{qj}^{(1)} &= f_{qj}^{(1)} - \tfrac{1}{4}\eta_j^{(3)}\delta_{q2} - \tfrac{1}{2}[\eta_j^{(1)} - \gamma_j^{(1)}]\,\delta_{q1} - \tfrac{1}{2}[\eta_j^{(1)} + \gamma_j^{(1)} - \tfrac{1}{2}\eta_j^{(3)}]\,\delta_{q0},\\
G_{qj}^{(0)} &= f_{qj}^{(0)} - \tfrac{1}{24}\eta_j^{(3)}\delta_{q3} - \tfrac{1}{8}[\eta_j^{(1)} - \gamma_j^{(1)}]\,\delta_{q2} - \tfrac{1}{2}[\eta_j^{(1)} + \gamma_j^{(1)} - \tfrac{3}{4}\eta_j^{(3)}]\,\delta_{q1}\\
&\quad - [\gamma_j^{(0)} + \tfrac{3}{8}\eta_j^{(1)} + \tfrac{5}{8}\gamma_j^{(1)} - \tfrac{1}{3}\eta_j^{(3)}]\,\delta_{q0},
\end{aligned}$$

where δ is the Kronecker delta, and

$$\eta_j^{(p)} = \sum_{q=0}^{J+4-p} f_{qj}^{(p)}, \quad \gamma_j^{(p)} = \sum_{q=0}^{J+4-p} (-1)^q f_{qj}^{(p)}.$$

REFERENCES

ACHENBACH, E. 1974 Vortex shedding from spheres. *J. Fluid Mech.* **62**, 209–221.

BATCHELOR, G. K. & GILL, A. E. 1962 Analysis of the stability of axisymmetric jets. *J. Fluid Mech.* **14**, 529–551.

FORNBERG, B. 1980 A numerical study of steady viscous flow past a circular cylinder. *J. Fluid Mech.* **98**, 819–855.

FORNBERG, B. 1988 Steady viscous flow past a sphere at high Reynolds numbers. *J. Fluid Mech.* **190**, 471–489.

FUCHS, H. V., MERCKER, E. & MICHEL, U. 1979 Large-scale coherent structures in the wake of axisymmetric bodies. *J. Fluid Mech.* **93**, 185–207.

GARBOW, B. S., BOYLE, J. M., DONGARRA, J. J. & MOLER, C. B. 1977 *Matrix Eigensystem Routines – EISPACK Guide Extension.* Springer.

GOLD, H. 1963 Stability of laminar wakes. PhD dissertation. Calif. Inst. Tech.

GOLDBURG, A. & FLORSHEIM, B. H. 1966 Transition and Strouhal number for the incompressible wake of various bodies. *Phys. Fluids* **9**, 45–50.

GOTTLIEB, D. & ORSZAG, S. A. 1977 *Numerical Analysis of Spectral Methods.* SIAM, Philadelphia.

HAMA, F. R. & PETERSON, L. F. 1976 Axisymmetric laminar wake behind a slender body of revolution. *J. Fluid Mech.* **76**, 1–15.

HAMA, F. R., PETERSON, L. F., VEAUX, S. C. DE LA & WILLIAMS, D. R. 1977 Instability and transition in axisymmetric wakes. *Proc. Conf. Laminar–Turbulent Transition.* AGARD-CP-224.

JACKSON, C. P. 1987 A finite-element study of the onset of vortex shedding in flow past variously shaped bodies. *J. Fluid Mech.* **182**, 23–45.

JAYAWEERA, K. O. L. F. & MASON, B. J. 1965 The behaviour of freely falling cylinders and cones in a viscous fluid. *J. Fluid Mech.* **22**, 709–720.

KAWAGUTI, M. 1955 The critical Reynolds number for the flow past a sphere. *J. Phys. Soc. Japan* **10**, 694–699.

KENDALL, J. M. 1964 The periodic wake of a sphere. *Space Programs Summary*, no. 37-25, vol. 4. Jet Propulsion Laboratory, Pasadena, CA.

KIM, H. J. & DURBIN, P. A. 1988 Observations of the frequencies in a sphere wake and of drag increase by acoustic excitation. *Phys. Fluids* **31**, 3260–3265.

KIM, I. 1989 Numerical study of the onset of instability in the flow past a sphere. Ph.D. dissertation, University of Arizona.

LESSEN, M. & SINGH, P. J. 1973 The stability of axisymmetric free shear layers. *J. Fluid Mech.* **60**, 433–457.

LIN, C. L., PEPPER, D. W. & LEE, S. C. 1976 Numerical methods for separated flow solutions around a circular cylinder. *AIAA J.* **14**, 900–907.

MACCREADY, P. B. & JEX, H. R. 1964 Study of sphere motion and balloon wind sensors. *NASA TM X*-53089.

MASLIYAH, J. H. 1972 Steady wakes behind oblate spheroids: flow visualization. *Phys. Fluids* **15**, 1144–1146.

MODI, V. J. & AKUTSU, T. 1984 Wall confinement effects for spheres in the Reynolds number range of 30–2000. *Trans. ASME* I: *J. Fluids Engng* **106**, 66–73.

MÖLLER, W. 1938 Experimentelle Untersuchengen zur Hydrodynamik der Kugel. *Phys. Z.* **39**, 57–80.

MONKEWITZ, P. A. 1988*a* The absolute and convective nature of instability in two-dimensional wakes at low Reynolds numbers. *Phys. Fluids* **31**, 999–1006.

MONKEWITZ, P. A. 1988*b* A note on vortex shedding from axisymmetric bluff bodies. *J. Fluid Mech.* **192**, 561–575.

MONKEWITZ, P. A. & NGUYEN, L. N. 1987 Absolute instability in the near-wake of two-dimensional bluff bodies. *J. Fluids Struct.* **1**, 165–184.

NAKAMURA, I. 1976 Steady wake behind a sphere. *Phys. Fluids* **19**, 5–8.

PETERSON, L. F. & HAMA, F. R. 1978 Instability and transition of the axisymmetric wake of a body of revolution. *J. Fluid Mech.* **88**, 71–96.

PREUKSCHAT, A. W. 1962 Measurements of drag coefficients for falling and rising spheres in free motion. Aeronautical engineering thesis, Calif. Inst. Tech.

PROVANSAL, M., MATHIS, C. & BOYER, L. 1987 Bénard–von Kármán instability: transient and forced regimes. *J. Fluid Mech.* **182**, 1–22.

ROOS, F. W. 1968 An experimental investigation of the unsteady flows about spheres and disks. PhD dissertation, University of Michigan.

ROOS, F. W. & WILLMARTH, W. W. 1971 Some experimental results on sphere and disk drag. *AIAA J.* **9**, 285–291.

SATO, H. & OKADA, O. 1966 The stability and transition of an axisymmetric wake. *J. Fluid Mech.* **26**, 237–253.

SEGUR, J. B. & OBERSTAR, H. E. 1951 Viscosity of glycerol and its aqueous solutions. *Ind. Engng. Chem.* **43**, 2117–2120.

SHAFRIR, U. 1965 Horizontal oscillations of falling spheres. AFCRL-65-141.

SHETH, R. B. 1970 Secondary motion of freely falling spheres. MS thesis, Brigham Young University.

STEEN, P. H. & AIDUN, C. K. 1988 Time-periodic convection in porous media: transition mechanism. *J. Fluid Mech.* **196**, 263–290.

STRINGHAM, G. E., SIMONS, D. B. & GUY, H. P. 1969 The behavior of large particles falling in quiescent liquids. US Geol. Survey Prof. Paper 562C.

TANEDA, S. 1956 Studies on wake vortices (III). Experimental investigation of the wake behind a sphere at low Reynolds numbers. *Rep. Res. Inst. Appl. Mech. Kyushu University* **4**, 99–105. (See also *J. Phys. Soc. Japan* **11**, 1104–1108.)

THOMAN, D. C. & SZEWCZYK, A. A. 1969 Time-dependent flow over a circular cylinder. *Phys. Fluids Suppl.* II, 76–87.

TOROBIN, L. B. & GAUVIN, W. H. 1959 Fundamental aspects of solids–gas flow. Part II. The sphere wake in steady laminar flow. *Can. J. Chem. Engng.* **37**, 167–176.

TOULCOVA, J. & PODZIMEK, J. 1968 Contribution to the question of the catching of aerosol particles in the wake of falling water droplets. *J. Rech. Atmos.* **3**, 89–95.

VIETS, H. 1971 Accelerating sphere–wake interaction. *AIAA J.* **9**, 2087–2089.

VIETS, H. & LEE, D. A. 1971 Motion of freely falling spheres at moderate Reynolds number. *AIAA J.* **9**, 2038–2042.

WILLMARTH, W. W., HAWK, N. E. & HARVEY, R. E. 1964 Steady and unsteady motions and wakes of freely falling disks. *Phys. Fluids* **7**, 197–208.

ZARIN, N. A. 1970 Measurement of non-continuum and turbulence effects on subsonic sphere drag. *NASA* CR-1585.

ZEBIB, A. 1984 A Chebyshev method for the solution of boundary value problems. *J. Comp. Phys.* **53**, 443–455.

ZEBIB, A. 1987 Stability of viscous flow past a circular cylinder. *J. Engng Maths.* **21**, 155–165.

ZIKMUNDOVA, J. 1970 Experimental investigation of the wake behind a sphere and a spheroid for Reynolds numbers from 44 to 495. *J. Rech. Atmos.* **4**, 7–18.